Microstructural and mechanical characterizations of Mo/W and Mo/graphite joints with BNi2 paste

*Biao Xu, Yuqi Cai, Julfikar Haider, Fahd Nawaz Khan, Tauheed Shehbaz, Hongyang Zhao, and Yangwu Mao**

B. Xu, Y. Q. Cai, Prof. H. Y. Zhao, Y. W. Mao
Hubei Key Laboratory of Plasma Chemistry and Advanced Materials, Wuhan Institute of Technology, Wuhan 430205, China
Email: **myw@wit.edu.cn**

J. Haider
Department of Engineering, Manchester Metropolitan University, Manchester M1 5GD, UK

F. N. Khan, T. Shehbaz
Faculty of Materials and Chemical Engineering, Department of Materials Science, Ghulam Ishaq Khan Institute of Engineering Sciences and Technology, Topi 23640, Pakistan

Y. W. Mao
Key Laboratory of Green Chemical Engineering Process of Ministry of Education, Wuhan Institute of Technology, Wuhan 430205, China

Key words: molybdenum, tungsten, brazing, microstructure, nanoindentation, BNi2

Brazing of Mo to W and to graphite have been achieved with BNi2 (containing Ni, Cr, Si and B) paste. For both the Mo/W and Mo/graphite joints, the joining area consists of a diffusion area and a brazing area. The diffusion area is composed of MoNi and Mo, formed by the diffusion of Mo substrate into the braze during brazing. The brazing area of the Mo/W joint contains Ni(ss) (solid solution), Cr(ss), Ni_3B, CrB and Ni_4W, while the brazing area of the Mo/graphite joint mainly comprises Ni(ss), MoNi, Ni_3B and CrB. For the Mo/graphite joint, a continuous chromium carbide layer is formed at the brazing area/graphite interface due to the reaction of Cr in the BNi2 braze with the graphite. The nanoindentation results of the joints show that the diffusion area exhibits the highest hardness and elastic modulus. The shear strengths of the Mo/W and Mo/graphite joints obtained are 58.1 ± 16.0 MPa and 13.0 ± 4.0 MPa, respectively. The Mo/W and Mo/graphite joints after shearing tests break in the W and

graphite sides close to the joining area, respectively, which suggests that both the fractures are caused by the stress concentration in the corresponding areas.

1. Introduction

Molybdenum (Mo) is exceedingly attractive in vacuum electronics and nuclear applications due to its good electrical and thermal conductivities, low coefficient of thermal expansion (CTE), excellent high temperature strength and high thermal shock resistance. [1] However, some practical applications of Mo require joining or integration with other materials. [2-6] For example, the fabrication of microwave tube in hot cathode component involves the joining of Mo to W. [7] In addition, the manufacturing of X-ray anode targets in computed tomography and angiography equipment includes the joining of Mo to graphite. [8]

Joining of Mo to W and to graphite have been conducted by diffusion bonding and brazing. [9-13] Wei et al. carried out Mo alloy/graphite diffusion bonding with a Zr interlayer at 1800°C and a pressure of 3 MPa. [9] The microstructural characterization revealed that the bonding area of the joint was mainly composed of Mo_2Zr, ZrC and (Zr, Mo)(ss) (solid solution). However, high pressure and high temperature as well as extended bonding time required in diffusion bonding may lead to a high-cost joining process.

Brazing is one of the prospective techniques for dissimilar materials joining owing to low cost and high reliability. [14] Sene and Motta brazed Mo to porous W with Ni-Mo filler at 1400°C and obtained the joint with tensile strength of 87.9 ± 0.5 MPa. [7] Lin et al. studied Mo/porous W brazing with a Pd foil at 1580~1640°C and with a Ti foil at 1680~1740°C, respectively. [10] Results showed that the Pd foil was more suitable for Mo/W brazing than the Ti foil. Fedotov et al. studied Mo/graphite brazing with Ti-Zr-Nb-Be powder filler at 1400°C with holding time of 20 min. [8] The joining area was mainly composed of β-(Ti,Mo)(ss), carbides (TiC and ZrC) and beryllide ($MoBe_2$ and $TiBe_2$). Lu et al. brazed Mo alloy to graphite at 1300~1700°C using fillers including Ti-56Ni, Ti-8.5Si, Ti-33Cr and Ti-30V-3Mo. [11] The results showed that the brazing area of joint with Ti-56Ni filler consisted of NiTi and Ni_3Ti, while (Ti,Mo)ss was formed at the Mo alloy/brazing area interface for the joints with Ti-8.5Si, Ti-33Cr and Ti-30V-3Mo fillers. Liu et al. studied Mo alloy/graphite brazing with Ti-40Cr filler at 1420~1510°C. The joint interface microstructure was Mo alloy/ Ti-Mo(Cr)/ Ti-Cr(Mo)/ TiC/ Cr_3C_2/ graphite. [12] Furthermore, Dong et al. studied Mo/graphite joining by vacuum arc pressure brazing with Ti-Zr filler at the pressure of 0.5~1 MPa and reported that the joint shear strength was 15.2 MPa. [13]

Though the study on the brazing of Mo to W and to graphite has been developed, there are

still some issues that need to be paid attention to. For instance, the brazing temperature used in Mo/W and Mo/graphite brazing is quite high (1400°C for Ni-Mo filler, 1610°C for Pd foil, 1400°C for Ti-Zr-Nb-Be filler, 1300~1700°C for Ti-56Ni, Ti-8.5Si, Ti-33Cr and Ti-30V-3Mo fillers, 1420~1510°C for Ti-40Cr filler), [7-8,10-12] which may lead to the high energy consumption and high cost of the processing. In addition, the use of relatively high pressure in brazing (0.5~1 MPa for pressure brazing technique) may cause the complexity of the brazing process. [13] Furthermore, the use of Ti-Zr-Nb-Be filler in Mo/graphite brazing may be limited due to the potential toxicity of Be. [8] Thus, it is essential and meaningful to study Mo/W and Mo/graphite brazing with a nontoxic filler at a relatively lower brazing temperature.

As a Ni-based commercial braze, BNi2 (mainly containing Ni, Cr, Si and B) braze has been used for high temperature dissimilar materials brazing because of its relatively low melting temperature (970~1000°C), environmentally friendliness and superior corrosion/oxidation resistance. Meanwhile, the active element Cr in the BNi2 braze may contribute to the improvement of wettability between the graphite and the braze. Thus, in this study the BNi2 paste was employed in brazing of Mo to W and to graphite. The microstructural and mechanical characterizations of the joints were performed.

2. Experimental Section

2.1. Materials

The brazing substrates in this study included pure Mo, W and graphite. The Mo substrate with an average density of 10.2 g cm^{-3}, a purity of 99.9 %, an average shear strength of 282.8 MPa and a size of 10 × 10 × 3 mm^3 was purchased from Shengze Metal Materials Company, Dongguan, China. The W substrate with an average density 19.2 g cm^{-3}, a purity of 99.9 % and a size of 10 × 10 × 5 mm^3 was acquired from Jinou Metal Materials Company, China. The graphite substrate with an average density of 1.9 g cm^{-3} and a size of 10 × 10 × 10 mm^3 was supplied by Jinglong Carbon Company, Beijing. Prior to brazing, the joining surfaces of the Mo, W and graphite substrates were polished by a 1000-grit SiC sandpaper to remove any impurities. Afterwards, the Mo, W and graphite substrates were ultrasonically cleaned in deionized water for 10 min and subsequently in ethanol for 30 min. The commercial BNi2 paste (7 wt.% Cr, 4.5 wt.% Si, 3 wt.% B, 3 wt.% Fe, Ni: balance) used for Mo/W and Mo/graphite brazing was provided by Höganäs China.

2.2. Brazing procedure

The brazing temperature was determined as 1060°C since the melting temperature of BNi2 paste was between 970°C and 1000°C. Brazing of Mo to W and to graphite were carried out

under a vacuum of 6×10^{-3} Pa in a molybdenum wire furnace. A schematic diagram of the Mo/W and Mo/graphite brazing assemblies is shown in **Figure 1**. A pressure of 4.7 kPa was applied to the brazing assembly to promote the interfacial bonding of the BNi2 paste with the substrates. The assemblies were heated at a rate of 10°C min^{-1} from room temperature to 500°C and kept at 500°C for 30 min for the volatilization and decomposition of the organic solvent in the BNi2 paste. Then the assemblies were further heated to 800°C at a rate of 10°C min^{-1} and subsequently heated to the brazing temperature of 1060°C at a rate of 5°C min^{-1}. The assemblies were cooled to room temperature by furnace cooling after brazing at 1060°C for 10 min.

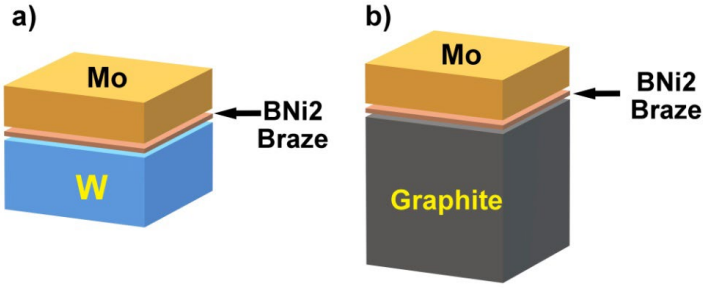

Figure 1. Schematic diagram of assemblies for Mo/W brazing a) and Mo/graphite brazing b) with BNi2 braze.

2.3. Microstructural characterization

The interfacial areas of the Mo/W and Mo/graphite joints were characterized by a field emission scanning electron microscopy (FESEM, GeminiSEM 300) and an energy dispersive spectroscopy (EDS, Oxford Inca X-Act). The phases of the interfacial areas of the Mo/W and Mo/graphite joints were identified by an X-ray diffraction (XRD, Bruker D8 Advance) using Cu Kα radiation with a wavelength of 0.15418 nm and an accelerating voltage of 40 kV at a scanning range of 10°~80°.

2.4. Mechanical characterization

Nanoindentation tests of the Mo/W and Mo/graphite joints were performed by a nanoindenter (iMicro, Nanomechanics). The nanohardness and elastic moduli at different regions of the joints were measured using a three-sided Berkovich tip with a maximum load of 10 mN. Each region of the joint was indented with a 2 × 2 grid. The load-displacement curves of nanoindentation were continuously monitored and recorded in a continuous stiffness mode.

Joint shear strengths were determined by the measurement illustrated by Cai et al. [15] **Figure 2** shows the schematic of shear strength tests for the Mo/W and Mo/graphite joints. The Mo/W and Mo/graphite joints were fixed in a jig and then an upper indenter was applied to the Mo parts in the joints at a rate of 0.5 mm min^{-1}. The shear strength was obtained by dividing the

maximum load of the upper indenter by the brazing area. The average joint strength was obtained based on at least five brazed samples.

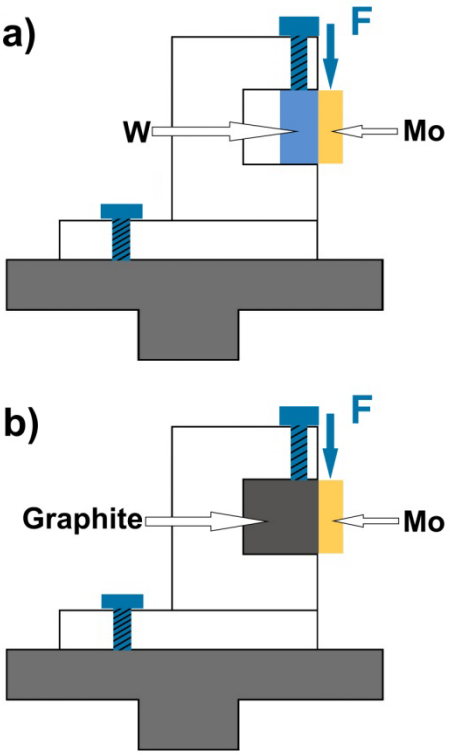

Figure 2. Schematic of shear strength tests for Mo/W a) and Mo/graphite b) joints.

3. Results and discussion

3.1. Microstructural characterization of Mo/W joint

Figure 3 shows micrograph and EDS mappings of the Mo/W joint brazed with BNi2 paste. Favorable interfacial bonding is achieved (neither microcracks nor pores), as can be seen in **Figure 3a**). The joining area is approximately 90 μm thick consisting of a brazing area and a diffusion area close to the Mo substrate. The diffusion area about 15~20 μm thick may be formed by the diffusion of Mo substrate into the liquid braze during brazing. The observation of a diffusion area between the Mo substrate and the filler area was also demonstrated by Chang and Shiue in Mo/Ti6Al4V brazing with Ti-Cu-Ni filler. [16] Liu et al. reported that a diffusion area was developed between the Mo interlayer and the filler in SiC/Kovar alloy brazing with Ni-Si filler and Mo foil. [17] The brazing area in the Mo/W joint contains dark-gray and light-gray regions. Moreover, a continuous black region can be distinguished in the brazing area close to the diffusion area side.

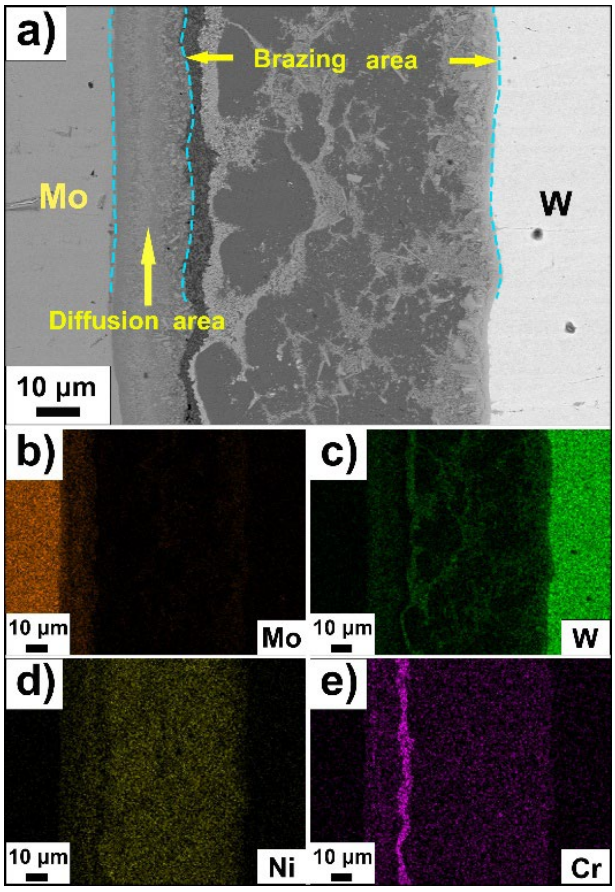

Figure 3. Micrograph a) and EDS mappings b-e) of the Mo/W joint with BNi2 paste.

The EDS mappings of the joint (**Figure 3b-e**) reveal that the diffusion area mainly contains elements Mo and Ni, confirming the diffusion of Mo into the liquid braze during brazing. The brazing area comprises Ni, Cr and W elements, but the element Cr enriches in the black region of the brazing area. Min et al. also observed the enrichment of Cr at the interface between the diffusion area and the brazing area in Mo/316L steel brazing with BNi2 braze. [18]

Figure 4 displays magnified micrographs of the joining area in the Mo/W joint. **Table 1** provides the EDS results of microzones marked in **Figure 4**. The microzone A in the diffusion area containing 44.31 at.% Mo and 39.57 at.% Ni is inferred as the mixture of MoNi and Mo. Liaw and Shiue demonstrated that a large amount of MoNi was formed by the reaction of Mo substrate with Ni in the filler in Mo/Mo brazing with Au-Ni-Pd filler. [19] The MoNi phase was also detected by Lin et al. in the Nb-Zr/Ti-Zr-Mo joint bonded with a Ni interlayer. [20] Min et al. reported that the diffusion area was composed of MoNi and Mo in the Mo/316L steel joint with BNi2 braze, which is consistent with the result in this study. [18]

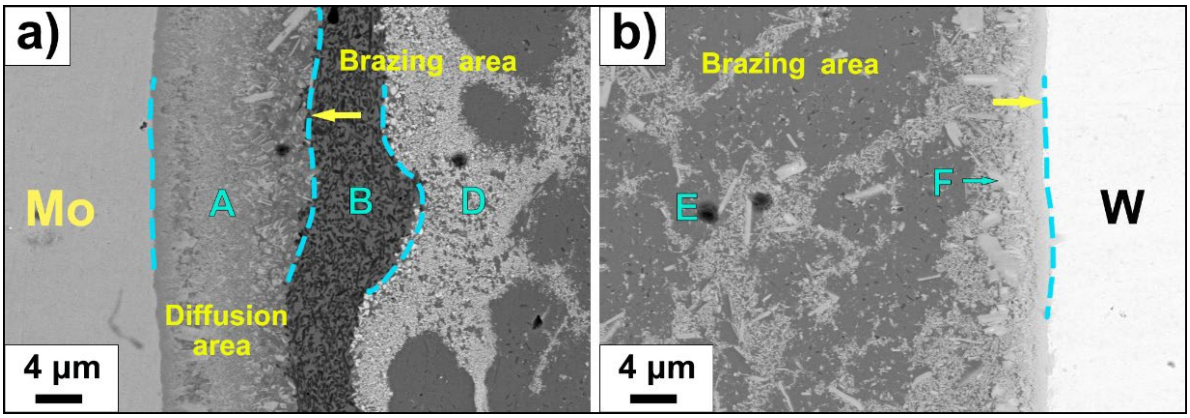

Figure 4. Magnified micrographs of the joining area in the Mo/W joint: a) Mo/diffusion area/brazing area part and b) brazing area/W part.

Table 1. EDS results of microzones in **Figure 4.**

Microzones	Compositions (at.%)						Possible phases
	Mo	W	Ni	Cr	Si	Fe	
A	44.31	0.31	39.57	14.19	0.64	0.98	MoNi, Mo
B	1.16	0.43	20.34	75.07	1.84	1.16	Cr(ss), Ni(ss)
D	3.33	8.89	70.84	9.11	6.98	0.85	Ni(ss), Ni-W
E	0.50	0.37	77.04	8.44	8.76	4.89	Ni(ss)
F	3.62	18.36	59.05	11.52	4.50	2.95	Ni-W

The black microzone B in the brazing area indicates 20.34 at.% Ni and 75.07 at.% Cr. Based on Ni-Cr phase diagram, Cr(ss) and Ni(ss) instead of Ni-Cr intermetallics can be formed. [21] Thus, the EDS result of the microzone B indicates that the black region in the brazing area mainly comprises Cr(ss) and Ni(ss). Peng demonstrated large solubility of Cr in the MoNi phase. [22] Therefore, the dissolved Cr in the MoNi phase may precipitate around the MoNi during the cooling process, resulting in the enrichment of Cr between the diffusion area and the brazing area. The light-gray microzone D in the brazing area shows high concentration of Ni (70.84 at.%) and a small amount of W (8.89 at.%), implying the formation of Ni(ss) and Ni-W intermetallics. The EDS result of the microzone E in the brazing area reveals the formation of Ni(ss) in the dark-gray regions. Wang et al. pointed out that Ni(ss) could be obtained by the interaction of Ni with Cr and Si atoms in the filler for brazing Mo to carbon-carbon (C-C) composite with Ni-Cr-Si-Ti filler. [23] The light-gray microzone F close to the W substrate contains 18.36 at.% W and 59.05 at.% Ni, determined as the Ni-W intermetallics. Zhong et al.

reported that Ni(W) solid solution and a small amount of Ni_4W were developed in the joining area in W/ferritic steel bonding with a Ni interlayer. [24]

Notably, element B in the BNi2 braze was not detected by EDS, probably due to its relatively small atomic number and amount. Jang and Shih claimed that element B was undetectable in EDS measurement; however, they declared that Ni_3B and CrB phases could be formed by the reaction of B with Ni and Cr in the BNi2 braze. [25] Nowacki reported neither boride formation nor element B detection for the steel/Fe–TiC joint with BNi2 braze. [26] Tillmann et al. pointed out that detection of element B was unavailable by EDS in the tool steel joint with BNi2 braze, however they confirmed that element B could be detected by using a glow discharge optical emission spectroscopy. [27]

For the Mo/W brazing with BNi2 paste, the following reactions may take place:

$$Mo + Ni = MoNi \quad (1)$$

$$4Ni + W = Ni_4W \quad (2)$$

$$3Ni + B = Ni_3B \quad (3)$$

$$Cr + B = CrB \quad (4)$$

The calculated value of ΔG (change of standard Gibbs free energy) for the reaction (1) was –106.286 kJ mol^{-1} at 1060°C, [28] indicating that the reaction of Mo with Ni could be spontaneous during the high temperature brazing. Based on the software HSC Chemistry Version 9 (Outotec Oyj, Finland), the ΔG values of the reactions (2), (3) and (4) at 1060°C are –16.043 kJ mol^{-1}, –71.635 kJ mol^{-1} and –69.485 kJ mol^{-1}, respectively, confirming the possibility to form Ni_4W, Ni_3B and CrB phases in the joining area.

Figure 5 shows the schematic, actual picture and XRD spectra of the plane in the Mo/W joint for XRD measurement. The W part in the joint was removed by cutting and then the obtained plane was measured with XRD. The XRD result reveals that phases including MoNi, Cr, Ni, CrB, Ni_4W, Ni_3B and Mo exist in the joint. Based on the results obtained by SEM and EDS, the diffusion area contains MoNi and Mo, and the brazing area comprises Ni(ss), Cr(ss) and Ni-W intermetallics. Thus, the detection of MoNi, Cr, Ni and Ni_4W in the XRD result is in accordance with the SEM and EDS analyses. Furthermore, the identification of CrB and Ni_3B suggests the reactions of both Cr and Ni with B in the BNi2 braze.

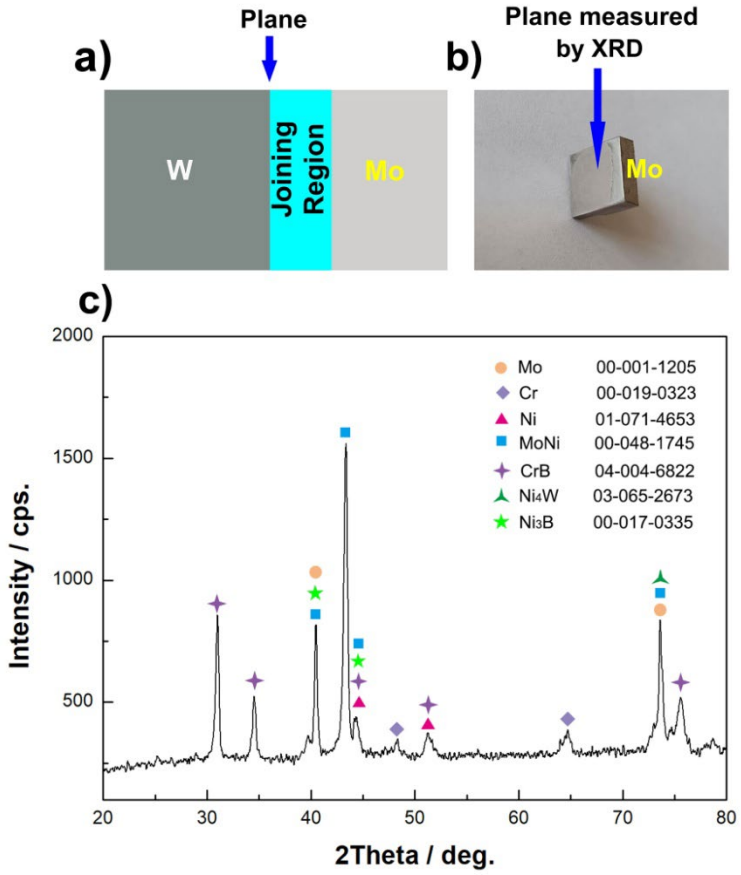

Figure 5. Schematic a), actual picture b) and XRD spectra c) of the plane in the Mo/W joint for XRD measurement.

Figure 6 shows the interface evolution in Mo/W brazing with BNi2 paste. At the heating stage (**Figure 6a**), the BNi2 braze starts to contact intimately with the Mo and W substrates under the applied load, after the paste undergoes the solvent volatilization and decomposition. When the temperature reaches to the liquidus line of the BNi2 braze, the braze begins to melt. At the braze melting stage (**Figure 6b**), the inter-diffusion of atoms occurs among the BNi2 filler, Mo and W substrates.

With further heating to the brazing temperature, the brazing assembly endures isothermal stage. At the isothermal stage (**Figure 6c**), a complete melting of the BNi2 braze takes place, resulting in an extensive inter-diffusion of the associated atoms. The diffusion of Mo substrate into the liquid braze followed by the interaction of Mo and Ni atoms results in formation of the MoNi-containing diffusion area near the Mo substrate. In the meantime, the diffusion of W substrate into the braze promotes the reaction of W with Ni atoms, resulting in the formation of Ni_4W in the liquid area close to the W substrate. In addition, partial Ni and Cr atoms react with B atoms in the liquid braze to form Ni_3B and CrB, respectively.

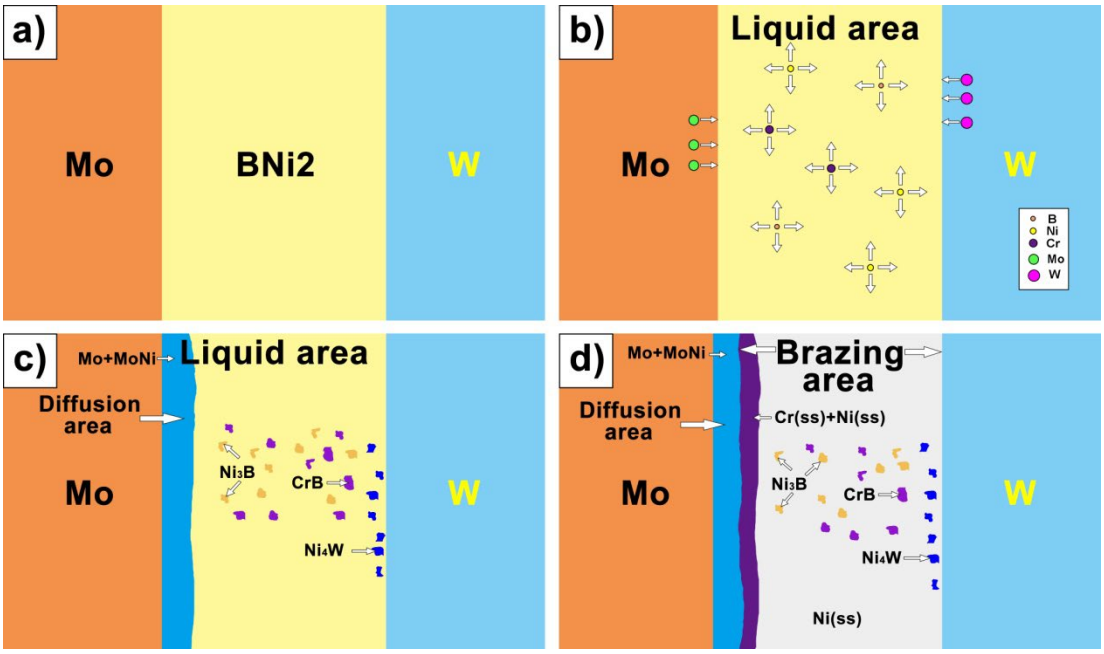

Figure 6. Interface evolution in Mo/W brazing with BNi2 paste: a) heating stage; b) braze melting stage; c) isothermal stage; d) cooling stage.

At the cooling stage (**Figure 6d**), the formed borides (Ni_3B and CrB) and Ni-W intermetallics can provide nucleation sites for the solidification of the liquid braze. The grains including Ni(ss) and Cr(ss) precipitate around the nucleation sites and then grow up in the brazing area. Thus, the brazing area was eventually composed of Ni(ss), Cr(ss), borides and Ni-W intermetallics.

3.2. Microstructural characterization of Mo/graphite joint

Figure 7 displays micrograph and EDS mappings of the Mo/graphite joint brazed with BNi2 paste. The FESEM image in **Figure 7a**) suggests sound interfacial bonding of the BNi2 braze with both the substrates. The joining area consists of a brazing area and a diffusion area adjacent to the Mo substrate, similar to that in the Mo/W joint. The thickness of the diffusion area (about 20 μm) is comparable to that in the Mo/W joint, whilst the thickness of the brazing area (about 40 μm) is less than that in the Mo/W joint, which may be caused by the infiltration of the liquid braze into the open pores of the graphite substrate.

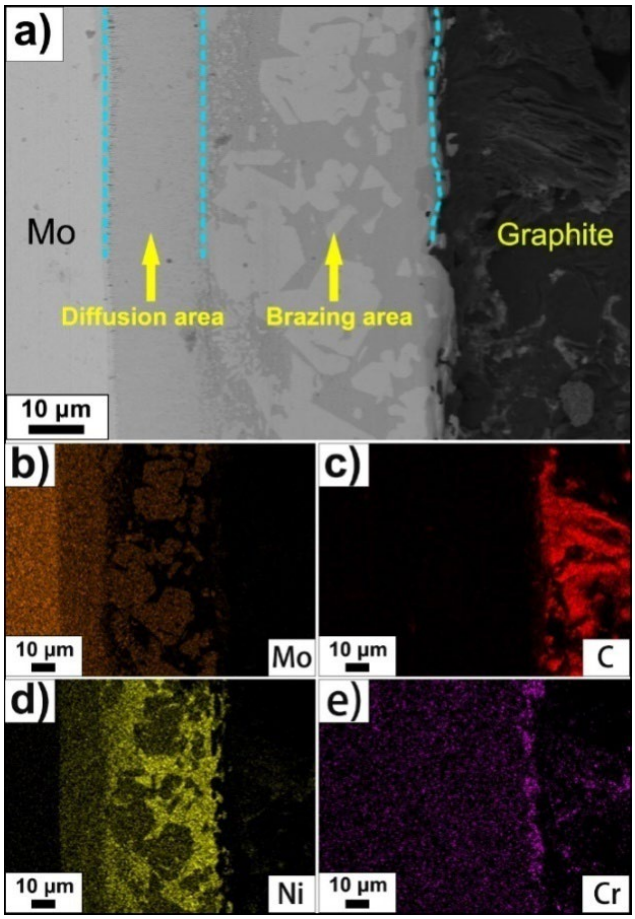

Figure 7. Micrograph a) and EDS mappings b-e) of the Mo/graphite joint with BNi2 paste.

The EDS mappings (**Figure 7b-e**) show that the diffusion area mainly comprises Mo and Ni elements, similar to that in the Mo/W joint. However, the brazing area in the Mo/graphite joint includes elements Mo, Ni and Cr, which is different from that in the Mo/W joint (mainly containing Ni and Cr). The existence of Mo in the brazing area in the Mo/graphite joint suggests the diffusion of Mo into the brazing area. Furthermore, element Cr enriches at the brazing area/graphite interface, implying the formation of chromium carbide by the reaction of Cr with the graphite substrate.

Figure 8 shows magnified micrographs of the joining area in the Mo/graphite joint. **Table 2** gives the EDS results of the microzones in **Figure 8**. The gray microzone G in the diffusion area near the Mo side contains 52.75 at.% Mo and 38.42 at.% Ni, inferred as the mixture of MoNi and Mo. This is in good agreement with the phase formation of the diffusion area in the Mo/W joint.

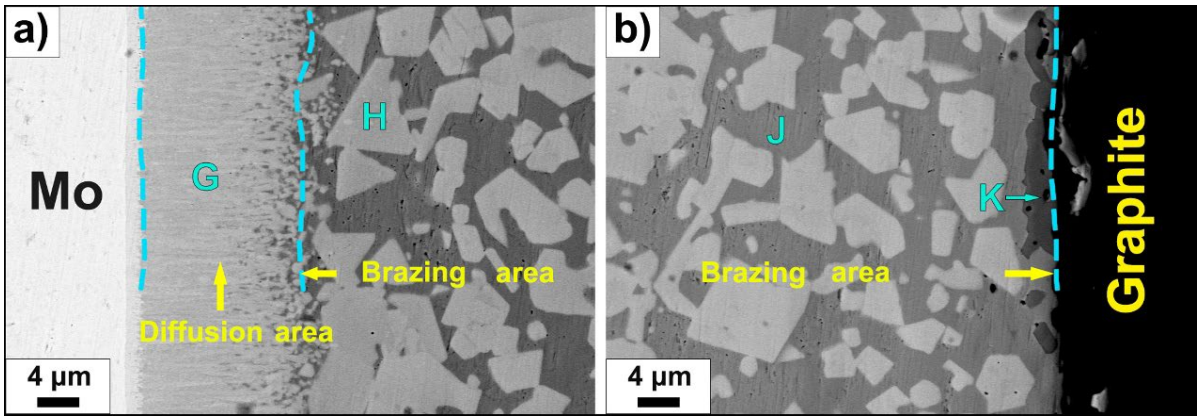

Figure 8. Magnified micrographs of the joining area in the Mo/graphite joint: a) Mo/diffusion area/brazing area part and b) brazing area/graphite part.

Table 2. EDS results of microzones in **Figure** 8.

Microzones	Compositions (at. %)						Possible phases
	Mo	C	Ni	Cr	Si	Fe	
G	52.75	-	38.42	6.69	1.83	0.31	MoNi, Mo
H	42.05	-	42.16	8.38	5.66	1.75	MoNi
J	13.33	-	76.22	6.36	3.48	0.61	Ni(ss), MoNi
K	4.76	40.89	0.75	53.40	-	0.20	Cr-C

The atomic ratio of Mo/Ni in the microzone H is close to 1:1, implying that the light-gray region in the brazing area is MoNi. The gray microzone J in the brazing area is mainly composed of 76.22 at.% Ni and 13.33 at.% Mo, suggesting the formation of Ni(ss) and MoNi. The dark-gray microzone K at the brazing area/graphite interface contains 40.89 at.% C and 53.40 at.% Cr, suggesting the formation of chromium carbide. Wang et al. reported that chromium carbide was developed at the C-C composite/brazing area interface due to high reactivity of carbon with Cr in Mo/C-C composite brazing with Ni-Cr-Si-Ti filler. [23] In addition, Zhang et al. illustrated that a continuous carbide layer, composed of Cr_3C_2 and Cr_7C_3, was formed at the graphite/brazing area interface in graphite/Cu brazing with Ni-Cr-P-Cu filler. [29] The ΔG values for the reactions ($3Cr + 2C = Cr_3C_2$ and $7Cr + 3C = Cr_7C_3$) at 1060°C are negative (–87.936 kJ mol^{-1} and –190.131 kJ mol^{-1}, respectively, calculated using the software HSC Chemistry Version 9), implying the possibility of chromium carbide (Cr_3C_2 and Cr_7C_3) formation.

Figure 9 displays the schematic, actual picture and XRD spectra of the plane in the

Mo/graphite joint for XRD measurement. The graphite part in the joint was removed by cutting and then the exposed metal-like plane was measured with XRD. The XRD spectra of the plane reveal the existence of phases including MoNi, Ni, Cr_3C_2, Cr_7C_3, Mo, C, CrB and Ni_3B. According to the SEM and EDS analysis, the diffusion area is mainly composed of MoNi and Mo, and the brazing area consists of Ni(ss), MoNi and borides. The detection of MoNi and Mo is related to the diffusion area. The identification of Ni, MoNi, CrB and Ni_3B corresponds to the brazing area. The detection of Cr_3C_2 and Cr_7C_3 confirms the chromium carbide formation at the graphite/brazing area interface. Furthermore, the carbon peaks in the XRD spectra are attributed to the residual graphite.

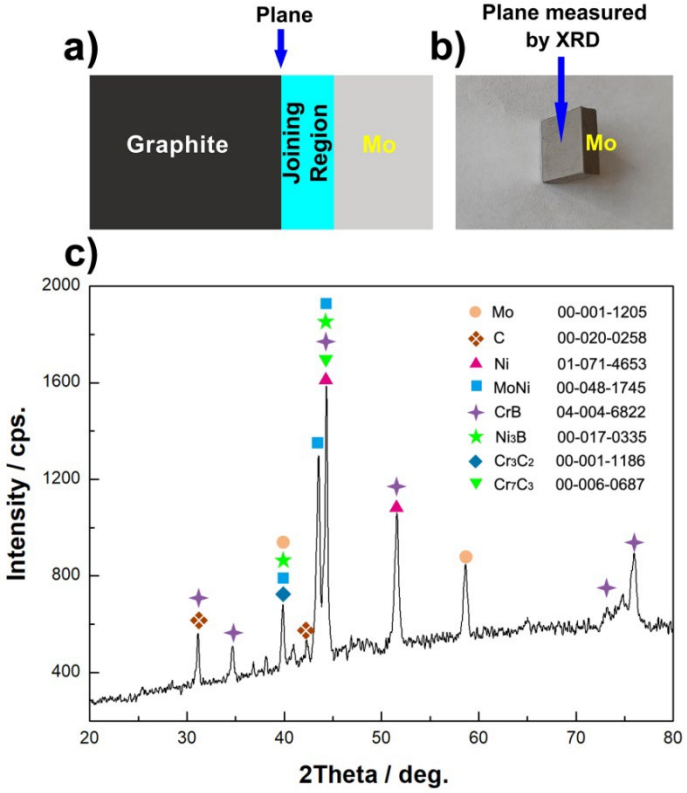

Figure 9. Schematic a), actual picture b) and XRD spectra c) of the plane in the Mo/graphite joint for XRD measurement.

3.3. Mechanical properties of joints

Figure 10 presents the nanoindentation load-displacement curves of the Mo/W and Mo/graphite joints. It can be seen that the diffusion areas of both the Mo/W and Mo/graphite joints show the lowest depth of penetration (about 115 nm and 130 nm, respectively), suggesting the least plastic deformation. The brazing areas in both the joints give the similar depth of penetration. The penetration depth of the Mo substrate is higher than that of W substrate, but much lower than that of graphite substrate. This implies that the plastic

deformation of Mo substrate is in the range between that of W and graphite substrates. It should be noted that the occurrence of discontinuities in the load-displacement curves of all areas can be associated to the dislocation activity, localized shearing and phase transformation occurring beneath the indenter tip. [30]

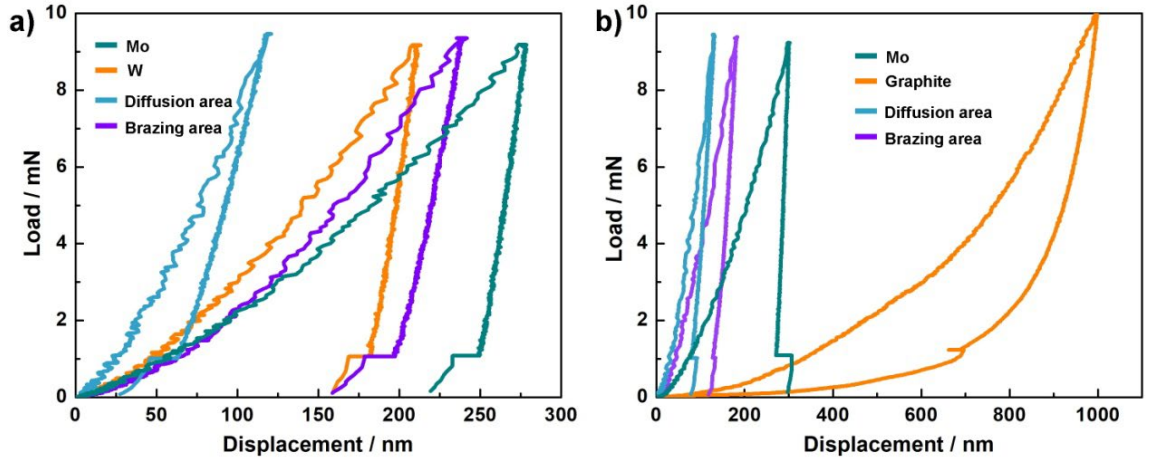

Figure 10. Nanoindentation load-displacement curves of Mo/W a) and Mo/graphite b) joints.

Nanohardness and elastic moduli of various areas in the Mo/W and Mo/graphite joints are shown in **Figure 11**. The hardness of Mo substrate in the Mo/W joint is 6.5 ± 0.3 GPa, similar to that in the Mo/graphite joint (6.2 ± 0.4 GPa). Yang et al. measured the nanohardness of Mo in Co/Mo multilayers as 7.1 GPa, close to the value in this study. [31] The elastic modulus of Mo substrate in the Mo/W and Mo/graphite joints is 361.6 ± 10.4 GPa and 352.3 ± 18.9 GPa, respectively, close to that (329 GPa) reported by Zhao et al. in C/SiC diffusion joining with a Mo-W-Mo interlayer. [32]

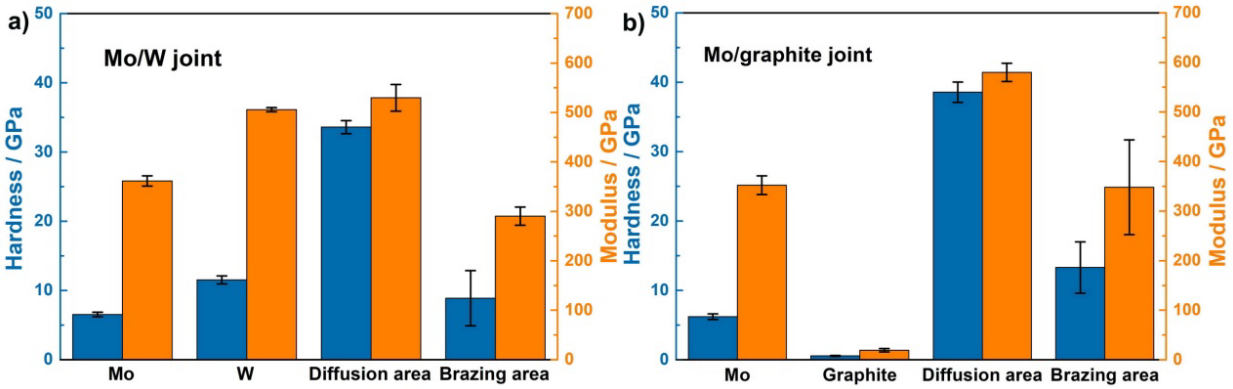

Figure 11. Nanohardness and elastic moduli of various areas in the Mo/W a) and Mo/graphite b) joints.

The nanohardness of W substrate in the Mo/W joint is 11.5 ± 0.6 GPa, consistent with that (11 GPa) reported by Gubisch et al. [33] The elastic modulus of the W substrate is 505.7 ± 4.2

GPa, comparable to that (300~ 500 GPa) measured by Moon and Han in tungsten film. [34] The nanohardness of graphite in the Mo/graphite joint is 0.6 ± 0.1 GPa, which is in good agreement with that (0.6 GPa) reported by Pradhan et al. [35] The elastic modulus of the graphite is 19.2 ± 3.5 GPa, higher than that of polycrystalline graphite (7~11 GPa). [36] This can be attributed to the residual stress existing in the graphite side due to thermal mismatch between the graphite and the filler. Pradhan et al. reported that the modulus of a graphite flake higher than that of polycrystalline graphite was attributed to the residual stress due to the surrounding matrix. [35]

The diffusion areas in the Mo/W and Mo/graphite joints exhibit the highest nanohardness (33.6 ± 0.9 GPa and 38.6 ± 1.5 GPa, respectively) and elastic modulus (529.7 ± 26.8 GPa and 579.9 ± 18.3 GPa, respectively), suggesting that the MoNi phase possesses the highest hardness and modulus in the joint. Min et al. also reported that the diffusion area (composed of MoNi and Mo) showed the highest microhardness in Mo/steel brazing with BNi2 paste. [18]

The nanohardness and elastic modulus of the brazing area in the Mo/W joint are 8.9 ± 4.0 GPa and 290.3 ± 18.4 GPa, respectively. Li et al. presented that the brazing area composed of Ni(ss) showed the nanohardness of 6 GPa and modulus of 137 GPa in the $Al_{0.3}$CoCrFeNi high-entropy alloy/FGH98 superalloy joint brazed with BNi2 filler. [37] Considering that the brazing area in the Mo/W joint contains not only Ni(ss) but also Cr(ss), borides and Ni-W intermetallics, higher hardness and modulus can be obtained. The hardness and elastic modulus of the brazing area in the Mo/graphite joint are 13.3 ± 3.7 GPa and 348.1 ± 95.5 GPa, respectively, both slightly higher than those in the Mo/W joint. This may be attributed to the presence of MoNi hard phase in the brazing area in the Mo/graphite joint.

Figure 12 displays the apparent shear strength and load-displacement curves of the Mo/W and Mo/graphite joints. The mechanical properties of joints are dependent on the microstructure of joints. As Min et al. demonstrated, the formation of the diffusion layer in Mo/316L steel brazing with BNi2 filler was favorable for the interfacial bonding, resulting in the shear strength improvement. [18] In addition, the formed borides (Ni_3B and CrB) in Ni(ss) may act as reinforcements in the Ni-based matrix composite, leading to the strengthening of the brazing area. The Mo/W joint exhibits the shear strength of 58.1 ± 16.0 MPa, comparable to that (55~92 MPa) obtained by De Prado et al. in the W/Eurofer joints brazed with 80Cu-20Ti filler. [38]

The shear strength of the Mo/graphite joint is 13.0 ± 4.0 MPa, much lower than that of the Mo/W joint, which is attributed to the weak graphite substrate with relatively low strength. However, the shear strength of the Mo/graphite joint is close to that of graphite substrate (15.2 ± 1.4 MPa), indicating the satisfactory bonding of the BNi2 braze with both the Mo and graphite substrates. Long et al. pointed out that the formed Cr_3C_2 and Cr_7C_3 at the diamond/filler layer

interface benefited for the solid bonding of the joint, thus promoting the joint strength. [39]

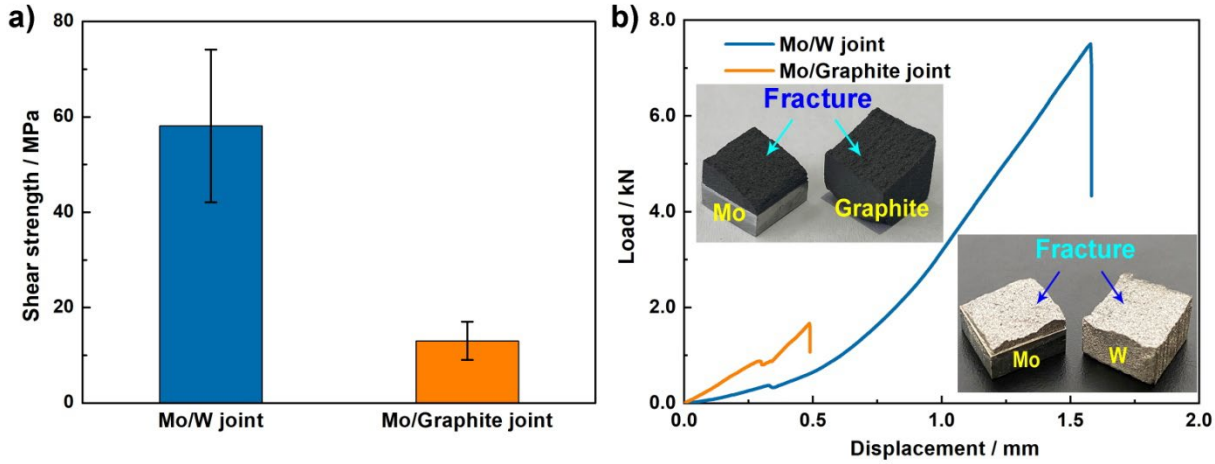

Figure 12. Apparent shear strength a) and load-displacement b) curves of Mo/W and Mo/graphite joints (inset: fracture images of Mo/W and Mo/graphite joints).

The fracture images of the Mo/W and Mo/graphite joints after shearing tests are shown in **Figure 12b)**, revealing that the Mo/W and Mo/graphite joints break in the W and graphite substrates close to the joining area, respectively. This implies that the fracture is caused by the stress concentration in the corresponding area due to the coefficient of thermal expansion (CTE) mismatch in the joints. The bowl-shape fracture also confirms the existence of residual stress in the joints. Considering that the CTE of W (4.3×10^{-6} K^{-1}) or graphite ($1.3\sim3.8 \times 10^{-6}$ K^{-1}) is lower than those of Mo (5×10^{-6} K^{-1}) and the BNi2 braze (13.4×10^{-6} K^{-1}), [40-43] higher joint stress can be concentrated in the W or graphite side close to the joining area. Liu et al. demonstrated that the fracture of W/steel joint with Ni–based filler and a Ta or Cu interlayer occurred in the W substrate close to the joining area, where the residual stress was concentrated. [44] Shang et al. also presented that the W/Fe-Ni-Co joints with Ag-27Cu-3.5Ti filler broke in the W side adjacent to the W/filler interface. [45]

4. Conclusions

1) Joining of Mo to W and to graphite have been achieved with BNi2 paste.
2) For both joints, the joining area consists of a diffusion area and a brazing area. The diffusion area mainly contains MoNi and Mo phases. The brazing area in the Mo/W joint is composed of Ni(ss), Cr(ss), Ni_3B and CrB together with Ni_4W close to the W substrate, while the brazing area in the Mo/graphite joint mainly comprises Ni(ss), MoNi, Ni_3B and CrB. Furthermore, a continuous chromium carbide layer is formed at the brazing area/graphite interface for the Mo/graphite joint.
3) The nanohardness and elastic moduli of various areas in the Mo/W and Mo/graphite joints

are obtained by nanoindentation tests. The diffusion area in both the joints exhibits the highest nanohardness and elastic modulus.

4) The shear strengths of the Mo/W and Mo/graphite joints are 58.1 ± 16.0 MPa and 13.0 ± 4.0 MPa, respectively. The Mo/W and Mo/graphite joints after the shearing tests break in the W and graphite sides close to the joining area, respectively, suggesting that the fracture is caused by the stress concentration in the corresponding area.

Acknowledgements

This work was supported by the National Natural Science Foundation of China (Grant No. 51304148) and by the WIT Graduate Education Innovation Fund (Grant No. CX2021164).

Conflicts of interest

The authors have no conflicts of interest to declare.

References

[1] S.P. Chakraborty, S. Banerjee, I.G. Sharma, A.K. Suri, *J. Nucl. Mater*. **2010**, *403*, 152.

[2] T. Zhao, D.F. Mo, X.M. Shi, W. Sun, X. Li, H.M. Gong, *Adv. Eng. Mater*. **2023**, in press. https://doi.org/10.1002/adem.202300964

[3] M.Y. Jia, F. Chen, L. Zhang, Z.F. Huang, Q. Shen, *J. Mater. Process. Technol*. **2022**, *302*, 117513.

[4] S. Maksymova, P. Kovalchuk, V. Voronov, *J. Mater. Eng. Perform*. **2023**, *32*, 5741.

[5] D.Y. Lin, J.X. Hu, X.G. Song, Z.X. Tang, Y.K. Wang, S.P. Hu, H. Bian, W. Fu, Y.Y. Song, *Mater. Charact*. **2023**, *204*, 113199.

[6] H.L. Feng, B. Chen, X.Y. Ren, H.S. Ren, W.W. Li, C. Pei, Y.W. Zhang, S.S. Li, W.J. Zou, H.P. Xiong, Y.Y. Cheng, *Int. J. Appl. Ceram. Technol*. **2023**, *20*, 2131.

[7] F.F. Sene, C.C. Motta, *Mater. Res*. **2013**, *16*, 417.

[8] I. Fedotov, A. Suchkov, A. Sliva, P. Dzhumaev, I. Kozlov, R. Svetogorov, O. Sevryukov, *J. Manuf. Processes* **2021**, *69*, 142.

[9] Y.N. Wei, H. Li, X. Peng, J.T. Zou, *Int. J. Refract. Met. Hard Mater*. **2020**, *92*, 105287.

[10] C.C. Lin, C.H. Shu, C. Chen, R.K. Shiue, H.J. Shy, *Int. J. Refract. Met. Hard Mater.* **2012**, *31*, 284.

[11] Q.B. Lu, W.M. Long, S.J. Zhong, J. Qin, Y.T. Jiu, H.W. Sun, *Weld. World* **2020**, *64*, 1877.

[12] D.G. Liu, J.X. Zou, P. Zhang, S.W. Zhou, H. Liu, Z.Q. Li, *Int. J. Refract. Met. Hard Mater*. **2023**, *115*, 106310.

[13] L.L. Dong, W.G. Chen, L.T. Hou, J.J. Wang, J.L. Song, *J. Mater. Process. Technol*. **2017**, *249*, 39.

[14] Y. Duan, Y.W. Mao, Z.M. Xu, Q.R. Deng, G.M. Wang, S.G. Wang, *Adv. Eng. Mater*. **2019**, *21*, 1900719.

[15] Y.Q. Cai, B. Xu, X.J. Ma, J. Haider, Y.W. Mao, S.G. Wang, *Arch. Civ. Mech. Eng.* **2023**, *23*, 58.

[16] C.T. Chang, R.K. Shiue, *Int. J. Refract. Met. Hard Mater*. **2005**, *23*, 161.

[17] G.W. Liu, F. Valenza, M.L. Muolo, A. Passerone, *J. Mater. Sci*. **2010**, *45*, 4299.

[18] M. Min, Y.W. Mao, Q.R. Deng, G.M. Wang, S.G. Wang, *Vacuum* **2020**, *175*, 109282.

[19] D.W. Liaw, R.K. Shiue, *Int. J. Refract. Met. Hard Mater*.**2005**, *23*, 91.

[20] J.M. Lin, Z.W. Yang, H.H. Wei, Y. Wang, Z.Q. Ma, D.P. Wang, *J. Alloys Compd.* **2018**, *743*, 780.

[21] H. Okamoto, M.E. Schlesinger, E.M. Mueller, *ASM Handbook Volume 3: Alloy Phase Diagrams*, ASM International **2016**.

[22] J. Peng, Doctor Thesis, *Karlsruhe Institute of Technology* **2016**.

[23] C. Wang, Q.G. Fu, W. Xie, Y.F. Ma, *Mater. Sci. Eng. A*. **2021**, *827*, 142014.

[24] Z.H. Zhong, H.C. Jung, T. Hinoki, A. Kohyama, *J. Mater. Process. Technol.* **2010**, 210, 1805.

[25] J.S.C. Jang, H.P. Shih, *J. Mater. Sci. Lett*. **2003**, *22*, 79.

[26] J. Nowacki, *Int. J. Mater. Prod*. **2008**, *33*, 291.

[27] W. Tillmann, T. Henning, M. Boretius, *Weld. World* **2019**, *63*, 1477.

[28] Y. Yu, C.P. Wang, Y.F. Li, X.J. Liu, R. Kainuma, K. Ishida, *Mater. Chem. Phys*. **2011**, *125*, 37.

[29] J. Zhang, T.P. Wang, C.F. Liu, Y.M. He, *Mater. Sci. Eng. A*. **2014**, *594*, 26.

[30] C.A. Schuh, *Mater. Today* **2006**, *9*, 32.

[31] G.H. Yang, B. Zhao, Y. Gao, F. Pan, *Surf. Coat. Technol*. **2005**, *191*, 127.

[32] X. Zhao, L.Y. Duan, W. Liu, Y.G. Wang, *Ceram. Int*. **2019**, *45*, 23111.

[33] M. Gubisch, Y. Liu, S. Krischok, G. Ecke, L. Spiess, J.A. Schaefer, C. Knedlik, *Tribol. Interface Eng. Ser*. **2005**, *48*, 409.

[34] M.W. Moon, J.H. Han, *Appl. Surf. Sci*. **2009**, *256*, 593.

[35] S.K. Pradhan, B.B. Nayak, S.S. Sahay, B.K. Mishra, *Carbon* **2009**, *47*, 2290.

[36] B.T. Kelly, *Physics of Graphite*, Applied Science Publisher **1981**.

[37] S.W. Li, J.L. Li, J.M. Shi, Y.J. Du, Y. Peng, F. Jin, J.T. Xiong, F.S Zhang, *Mater. Sci. Eng. A*. **2021**, *804*, 140714.

[38] J. de Prado, M. Sánchez, A. Ureña, *Fusion Eng. Des.* **2017**, *124*, 1082.

[39] F. Long, P. He, D.P. Sekulic, *Met.* **2018**, *8*, 315.

[40] G. Grabowski, Z. Pędzich, *J. Eur. Ceram. Soc*. **2007**, *27*, 1287.

[41] F. Cardarelli, *Ceramics, Refractories, and Glasses. In: Materials Handbook,* Springer, Cham, **2018**.

[42] G.Q. Chen, J.P. Liu, X. Shu, B.G. Zhang, J.C. Feng, *Vacuum* **2018**, *154*, 1.

[43] Y. Luo, W.C. Jiang, Q. Zhang, W.Y. Zhang, M.M. Hao, *Int. J. Hydrogen Energy* **2016**, *41*, 7464.

[44] W.S. Liu, Z.X. Wang, Y.Z. Ma, Q.S. Cai, *Fusion Eng. Des*. **2016**, *113*, 102.

[45] J.L. Shang, J.Z. Yan, N. Li, *J. Alloys Compd*. **2014**, *611*, 91.